


Article

Takagi–Sugeno Fuzzy Parallel Distributed Compensation Control for Low-Frequency Oscillation Suppression in Wind Energy-Penetrated Power Systems

Ruikai Song ¹, Sunhua Huang ^{2,*}, Linyun Xiong ^{1,*}, Yang Zhou ³ , Tongkun Li ¹, Pizheng Tan ¹ and Zhaozun Sun ¹

- ¹ School of Electrical Engineering, Chongqing University, Chongqing 400044, China; 202211021040@stu.cqu.edu.cn (R.S.); 202311021086t@stu.cqu.edu.cn (T.L.); 202311021028@stu.cqu.edu.cn (P.T.); 202311021002@stu.cqu.edu.cn (Z.S.)
- ² Department of Electrical and Electronic Engineering, The Hong Kong Polytechnic University, Hong Kong 999077, China
- ³ State Key Laboratory of Disaster Prevention & Reduction for Power Grid, Changsha University of Science & Technology, Changsha 410114, China; yangzhou@csust.edu.cn
- * Correspondence: sunhua.huang@polyu.edu.hk (S.H.); 1669554200@cqu.edu.cn (L.X.)

Abstract: In this paper, a Takagi–Sugeno fuzzy parallel distributed compensation control (TS-PDCC) is proposed for low-frequency oscillation (LFO) suppression in wind energy-penetrated power systems. Firstly, the fuzzy C-mean algorithm (FCMA) is applied to cluster the daily average wind speed of the wind farm, and the obtained wind speed clustering center is used as the premise variable of TS-PDCC, which increases the freedom of parameter setting of the TS fuzzy model and is closer to the actual working environment. Secondly, based on the TS fuzzy model, the TS-PDCC is designed to adjust the active power output of the wind turbine for LFO suppression. To facilitate the computation of controller parameters, the stability conditions are transformed into a set of Linear Matrix Inequalities (LMIs) via the Schur complement. Subsequently, a Lyapunov function is designed to verify the stability of the wind energy-penetrated power system and obtain the parameter ranges. Simulation cases are conducted to verify the validity and superior performance of the proposed TS-PDCC under different operating conditions.

Keywords: low-frequency oscillation; wind energy penetration; TS fuzzy model; fuzzy C-mean algorithm; parallel distributed compensation



Citation: Song, R.; Huang, S.; Xiong, L.; Zhou, Y.; Li, T.; Tan, P.; Sun, Z. Takagi–Sugeno Fuzzy Parallel Distributed Compensation Control for Low-Frequency Oscillation Suppression in Wind Energy-Penetrated Power Systems. *Electronics* **2024**, *13*, 3795. <https://doi.org/10.3390/electronics13193795>

Academic Editor: Ahmed Abu-Siada

Received: 16 August 2024

Revised: 18 September 2024

Accepted: 20 September 2024

Published: 25 September 2024



Copyright: © 2024 by the authors. Licensee MDPI, Basel, Switzerland. This article is an open access article distributed under the terms and conditions of the Creative Commons Attribution (CC BY) license (<https://creativecommons.org/licenses/by/4.0/>).

1. Introduction

The development of renewable energy and low carbon transformation of modern power systems has great strategic importance for resolving the energy crisis and releasing the issue of pollution [1–3]. Renewable energy is more economical and environmentally friendly than traditional energy sources, resulting in an increasing share of renewable energy in power systems worldwide [4,5]. Among all the renewable energy sources (RESs), wind energy has taken a dominant role in modern power systems. Different wind turbine structures are being utilized in both the commercial and academic arena, i.e., squirrel-cage induction generator, permanent magnetic synchronous generator, and doubly fed induction generator (DFIG), to name a few [6]. Among these wind turbines, the DFIG has gained more attention due to its structural simplicity, higher efficiency, and economic superiority.

However, the structure of a DFIG is different from a synchronous generator (SG). The difference is mainly reflected in the weak coupling between the rotor and stator of the DFIG [7,8], making the DFIG show weak damping characteristics. In addition, to maintain the stability of the grid-side voltage of the DFIG, the implementation of phase-locked loops exacerbates the weak damping characteristic and further deteriorates system damping levels [9–11]. Consequently, the integration of a significant number of

DFIGs into the power system to replace SGs may lead to varying degrees of weakening in the system's inertia, operating characteristics, and damping characteristics. Moreover, considering the remoteness of the wind resources required for DFIG generation, long-distance transmission lines are typically employed between wind farms and the grid, which reduces the damping ratio of interregional low-frequency oscillation (LFO) and increases the interregional instability risk factor in wind energy-penetrated power systems [12–15]. As the need for global-level energy transmission escalates and the installation of DFIGs skyrockets across the globe, LFO issues become increasingly prevalent. Hence, the study of strategies to suppress LFO in wind energy-penetrated power systems holds paramount practical significance.

Existing studies on LFO for wind energy-penetrated power systems mainly focus on oscillation mechanisms and suppression measures. With regard to LFO mechanism research, a new electromechanical oscillation-based theory is proposed in [16], which suggests that some of the oscillations are generated by the interaction of the new energy device with the slower-reacting parts of the power system. Furthermore, a damping torque analysis method is proposed in [17], which analyzes the load flow variations induced by the DFIG grid connection and the dynamic interaction between a DFIG and an SG. In [18], the damping control mechanism for a DFIG is investigated through an analysis of the influence of inertia control on LFO characteristics in a four-machine, two-area system. Apart from that, the influence of control on multiple-mode LFO is evaluated through eigenvalue sensitivity analysis in [19,20]. In order to eliminate the influence of non-dominant oscillation modes on the localization of the oscillatory source and to realize the precise positioning of the oscillatory source, an energy function-based LFO oscillatory source tracking approach is proposed in [21]. Other than that, the mechanism of wind turbine droop control on system stability under small disturbances is analyzed in [22,23]. However, the research on LFO mechanisms mentioned above is primarily based on mathematical modeling, which becomes challenging for numerical computation due to the expansion of the grid scale and the increase in nonlinear energy devices. In addition, due to the complexity of the grid model and power electronic devices, mathematical modeling is mainly applied in offline analysis after an LFO incident occurs, making it difficult to adopt for real-time LFO suppression.

With respect to the aspect of LFO suppression, various damping controls have been proposed to suppress LFO in conventional power systems, where power system stabilizers (PSSs) are most widely applied [24,25]. However, since traditional SG-PSS is primarily designed based on local area parameters, the unique geographical distribution of wind resources necessitates long-distance transmission from wind farms, which negatively impacts the effectiveness of existing PSS control strategies in suppressing inter-area oscillations. Additionally, a traditional PSS relies on local input signals, limiting its ability to fully observe the oscillation modes of the entire system, while communication delays further undermine the overall effectiveness of LFO suppression [26,27]. In order to overcome the problem of ineffective suppression of PSSs between areas, a wide-area data measurement scheme is presented in [28]. Although deploying multiple Wide Area Measurement Systems-based PSSs can, to some extent, alleviate the interregional LFO in DFIG-based power systems, it requires the grid to contain a large number of SGs for PSS installation and needs the allocation of a high amount of investment. As the number of PSSs declines due to the replacement of SGs with RESs, the utilization of DFIGs to achieve LFO suppression has been widely studied. In order to realize LFO damping by DFIGs, power oscillation dampers (PODs) are installed on DFIGs in [16]. A two-stage damping control scheme is adopted in [29] to enhance the damping characteristics of the wind turbine by controlling the torsional oscillation damping. Considering the relationship between the control parameters and the oscillation modes, an LFO suppression method that takes into account the frequency regulation by modeling the energy curvature has been proposed in [30]. A curvature-based control method is proposed to enhance the dynamic performance of low-inertia power systems in [31]. Furthermore, a taxonomy of power converter control schemes based on the

concept of complex frequency is proposed in [32]. The disturbance rejection capability of DFIG-based systems suffering from oscillations is enhanced by the introduction of virtual inertia control technology in [33]. Regarding the issue of distributed control, the Artstein transformation is utilized to convert a power system with communication delays into a delay-free model in [34]. Simultaneously, a saturation compensation system is employed to design external inputs, thereby enhancing the transient stability of the power system. In [35], a robust distributed timing fault-tolerant controller based on power sharing is proposed, and the convergence speed is further improved by observing the average voltage of the generator through a distributed fixed-time observer. A fixed-time fractional-order sliding mode controller is utilized for wind turbine control to improve power quality in [36]. Additionally, communication delays are mitigated through state transformation, and a saturation timing controller based on the hyperbolic tangent function is used to alleviate the effects of saturation in [37].

Nevertheless, there are several key issues in the above studies [24–33]. First of all, if the scheme of increasing the number of PSS and POD installations is used to suppress LFO, it will increase the construction cost, and the maintenance of related equipment in long-term operation will also reduce the economic benefits of wind farms. In addition, as the proportion of renewable energy equipment gradually increases, the effectiveness of the installed PSS and POD devices in suppressing LFO will be weakened. As a result, it will be difficult for the original devices to effectively suppress LFO when PSS and POD devices cannot be continuously invested. Secondly, it is difficult for the existing modeling scheme to cope with the increasing number of renewable energy devices in the power system, which is caused by the nonlinearity of renewable energy devices and the complexity of large-scale power systems. Therefore, the system model is changed when new devices are connected, making the original control strategy unable to suppress the LFO when the change in the system model exceeds a critical value.

In order to overcome the above issues, a novel LFO suppression strategy for DFIG-based power systems is investigated using a fuzzy C-mean algorithm (FCMA), TS fuzzy model, and TS parallel distributed compensation control (TS-PDCC) in this paper. In addition, Lyapunov functions are used in this paper to determine the stability of the control strategy. The main contributions of this paper are as follows:

- (i). The TS fuzzy approach is used to model the wind energy-penetrated power system with DFIGs, and the ability of the TS fuzzy model to approximate the nonlinear model is exploited to avoid the problem of computational difficulties that occur in large-scale RES-based power systems.
- (ii). A novel premise variable processing method of the TS fuzzy model is proposed to form TS fuzzy sets by clustering the daily average wind speeds by adopting an FCMA, which solves the problems of the loss of information of the TS fuzzy model. Additionally, the problem of unsolvable Linear Matrix Inequalities (LMIs) in controller parameter design is improved.
- (iii). Based on the FCMA premise of variable processing, a novel TS-PDCC strategy is proposed. Compared with the traditional control methods, the proposed control strategy improves the accuracy of the control effect through a high-fit TS fuzzy model, which presents a superior performance in reducing the amplitude of system oscillations and shortening the duration of oscillations.

Based on the aforementioned theoretical contributions, the TS-PDCC proposed in this paper offers the following practical contributions to real power systems. Firstly, the excellent performance of TS-PDCC in LFO suppression effectively enhances the stability of wind-integrated power systems, ensuring the security and reliability of renewable energy grids. Secondly, TS-PDCC does not require additional suppression devices, making its construction cost lower than that of existing PSS and POD schemes, thereby reducing wind farm construction costs and promoting wind farm development and grid integration. Finally, the capacity of TS-PDCC to handle complex nonlinearities effectively addresses the challenges of system nonlinearity and power system complexity arising from the increasing

number of renewable energy devices, improving the feasibility of applying renewable energy sources, such as wind power, in power systems.

The remainder of this paper will be organized as follows: Section 2 will introduce the theoretical background of wind energy-penetration systems, low-frequency oscillations, and parallel distributed compensation control; in Section 3, the TS fuzzy-based power system model with wind farms will be constructed; Section 4 will present the design and stability proof of the TS-PDCC controller; simulation analyses will be conducted in Section 5; and finally, the paper will be concluded in Section 6.

2. Theoretical Background

2.1. Energy Systems with Wind Penetration

As wind power takes up an increasingly larger proportion of the power system, a characteristic of high wind energy penetration in the power grid has gradually emerged, significantly altering the operational dynamics of the grid. Traditional power systems rely on synchronous generators to provide system inertia and damping. However, in high wind energy-penetration systems where wind turbines, such as DFIGs, dominate, their weak coupling characteristics make it difficult to provide effective damping and inertia support. Consequently, in power systems with high wind energy penetration, the overall system inertia decreases, leading to increased sensitivity to disturbances, especially during faults or load shedding, making the system more prone to low-frequency oscillations.

The active power output expression of the DFIG is as follows:

$$P_w = \frac{1}{2} \rho v^3 Y C_p \quad (1)$$

where ρ denotes the air density; v indicates the wind speed; Y represents the area of the swept plane of the rotor; and C_p is the power coefficient of wind energy utilization.

From Equation (1), it can be deduced that the active power output of the wind turbine depends on C_p when the wind speed is constant. C_p has a nonlinear relationship with wind speed, rotor speed, rotor radius, and pitch angle, and can be calculated using the following equation:

$$\begin{cases} C_p = 0.5176 \left(\frac{116}{\eta_i} - 0.4\beta - 5 \right) e^{-\frac{21}{\eta_i}} + 0.0068 \frac{\omega_m R}{v} \\ \eta_i = \left(\frac{1}{\frac{\omega_m R}{v} + 0.08\beta} - \frac{0.035}{\beta^3 + 1} \right)^{-1} \end{cases} \quad (2)$$

where β represents the pitch angle; ω_m denotes the rotor speed of the wind turbine; and R indicates the radius of the wind turbine rotor.

From Equations (1) and (2), it can be deduced that under a fixed pitch angle β , adjusting the rotor speed ω_m of the wind turbine according to the wind speed can maximize the power coefficient C_p , thereby achieving optimal wind energy utilization, known as the maximum power point tracking control mode. However, although the wind turbine maximizes its power capture under the maximum power point tracking mode, it cannot reserve active power to participate in the suppression of LFO. Therefore, to improve the stability of wind energy-penetration systems, power regulation of the wind turbine is necessary during LFO events to provide virtual inertia and damping, thereby suppressing oscillations through the active power changes of the DFIG.

2.2. Low-Frequency Oscillation

Low-frequency oscillation refers to the oscillation phenomenon in power systems caused by weak coupling or power exchange between generator rotors, typically occurring in the range of 0.1 to 2.5 Hz. In traditional power systems dominated by synchronous generators, inertia and damping characteristics effectively suppress LFO through excitation

system adjustments. The dynamics of low-frequency oscillations can be described by the following equations:

$$\begin{cases} \frac{d\delta}{dt} = \omega \\ \frac{d\omega}{dt} = \frac{P_m - P_e}{2M} \end{cases} \quad (3)$$

where δ represents the rotor angle of the generator, ω is the rotor angular velocity, P_m is the mechanical input power, P_e is the electrical output power, and M is the inertia time constant. From Equation (3), the system's inertia constant M determines the system's response speed to frequency changes. A larger inertia constant M can effectively mitigate frequency fluctuations and help maintain system stability.

The equivalent inertia M_{eff} of a high wind energy-penetration system can be expressed by the following equation:

$$M_{eff} = \frac{\sum_{i=1}^n M_i S_i}{\sum_{i=1}^n S_i} \quad (4)$$

where M_i and S_i represent the inertia constant and capacity of the i -th generation unit, respectively. Therefore, as low-inertia wind turbines gradually replace traditional synchronous generators, the equivalent inertia of the high wind energy-penetration system will decrease according to Equation (4), leading to insufficient damping for suppressing LFO in the system.

In addition, wind farms are usually located in remote areas far from load centers and are connected to load centers through long-distance transmission lines. This long-distance transmission further reduces the damping effect of the system, making power exchange between regions more unstable, which is likely to trigger more significant low-frequency oscillations. The impedance of long-distance transmission lines increases the phase angle difference in the system, further exacerbating oscillations. Power exchange in AC transmission systems can be described as follows:

$$P = \frac{V_1 V_2}{X} \sin \delta \quad (5)$$

where V_1 and V_2 represent the voltages at the two ends of the bus, X is the line reactance, and δ is the phase angle difference between the two voltages. The large reactance X of long-distance transmission lines results in more significant changes in the phase angle difference δ , thereby further exacerbating the risk of low-frequency oscillations in high wind energy-penetration systems.

2.3. Parallel Distributed Compensation Control

Parallel distributed compensation control is a strategy commonly used for controlling nonlinear systems and is widely applied in fuzzy control systems. The main idea of PDC is to divide a nonlinear system into several locally linearized subsystems and then design independent controllers for each subsystem. These local controllers are weighted through fuzzy inference to form a global controller, thereby achieving effective control over the entire nonlinear system.

Nonlinear systems are usually difficult to control accurately using traditional linear control methods. Therefore, PDC proposes a distributed compensation control method based on fuzzy rules. Consider a nonlinear system whose state equation is as follows:

$$\dot{x}(t) = f(x(t), u(t)) \quad (6)$$

where $x(t)$ is the system state, $u(t)$ is the control input, and $f(x(t), u(t))$ is the nonlinear function describing the system dynamics. For nonlinear systems, it is very difficult to directly design a global controller. Therefore, PDC divides the system into multiple locally

linearized subsystems, each of which can be approximately described by the following linear model:

$$\begin{aligned} &\text{if rule } i \text{ is active} \\ &\dot{x}(t) = A_i x(t) + B_i u(t) \end{aligned} \quad (7)$$

where A_i and B_i are the system matrices of the local linear model, representing the system's dynamic behavior under fuzzy rule i . When the fuzzy system is represented by multiple "IF-THEN" rules, the fuzzy controller uses the membership function $\mu_i(x)$ to weight and sum the different local models, forming the following global controller:

$$\dot{x}(t) = \sum_{i=1}^N \mu_i(x) (A_i x(t) + B_i u(t)) \quad (8)$$

where N is the total number of fuzzy rules. Control over the entire nonlinear system is achieved through Equation (8).

3. Fuzzy System Modeling

3.1. Methodological Approach

The proposed study aims to suppress LFO in high wind energy-penetration power systems using the TS fuzzy model and parallel distributed compensation control strategy. The specific research methodology is divided into the following steps:

(1) Wind Speed Data Collection

First, historical daily average wind speed data are obtained from wind farms. The daily average wind speed data reflects the wind speed variations over different periods and represents the typical wind speed characteristics of the wind farm throughout the year. Therefore, by analyzing the wind speed data, the long-term operational conditions of the wind farm and wind speed fluctuations can be captured, providing a data foundation for subsequent analysis.

(2) Wind Speed Data Clustering

Next, establishing corresponding fuzzy sets for too many wind speed ranges would result in an excessive number of fuzzy rules in the TS fuzzy model, making it difficult to solve the controller parameters. Therefore, the FCM algorithm is used to cluster the wind speed data into four categories (i.e., low wind speed, medium wind speed, high wind speed, and very high wind speed). These four characteristic wind speeds serve as the antecedent variables in the subsequent TS fuzzy model, representing the typical operating conditions of the wind farm.

(3) Subsystem Modeling

For each characteristic wind speed, a power system state equation that includes the wind farm is established. The state equation of each subsystem describes the dynamic behavior of the power system under that specific wind speed condition. Through these state equations, the proposed control strategy can capture the dynamic characteristics and responses of the power system under different wind speeds, including changes in voltage, frequency, active power, and reactive power. Therefore, the nonlinear behavior of the system is decomposed into multiple controllable linear subsystems.

(4) Fuzzy Rule Construction

Based on the characteristic wind speeds and the corresponding subsystem state equations, a set of fuzzy rules is constructed. The characteristic wind speeds are used as the antecedents of the fuzzy rules, while the subsystem state equations serve as the consequents. Each fuzzy rule describes the dynamic response of the system under different wind speed conditions.

(5) Global TS Fuzzy Model Construction

All subsystems are connected through Gaussian membership functions to form a global TS fuzzy model. The Gaussian membership functions define smooth transitions between different wind speed ranges, allowing the system to dynamically adjust its response under various wind speed conditions. In this way, a global fuzzy model that can

dynamically adapt to wind speed changes is constructed, accurately capturing the complex dynamic characteristics of a high wind energy-penetration system.

(6) Parallel Distributed Compensation Controller Design

For each subsystem, an independent feedback controller is designed, with the control input being the active power output of the DFIG. Using the same fuzzy rules and membership functions as the TS fuzzy model, a global controller is designed to ensure effective suppression of LFO under different wind speed conditions, and the parameters are solved through LMIs. The design of the feedback controllers is primarily aimed at the dynamic characteristics of each subsystem, providing appropriate control signals to stabilize the system's dynamic response.

(7) Low-Frequency Oscillation Suppression

The global controller is integrated into the active power control loop of the DFIG. When LFO occurs in the system, the active power output of the DFIG is adjusted to provide virtual inertia and damping, thereby suppressing low-frequency oscillations. By controlling the active power output of the DFIG, the wind turbine can effectively participate in LFO suppression in high wind energy-penetration power systems, enhancing the overall stability of the system.

The flowchart of the research methodology is shown in Figure 1.

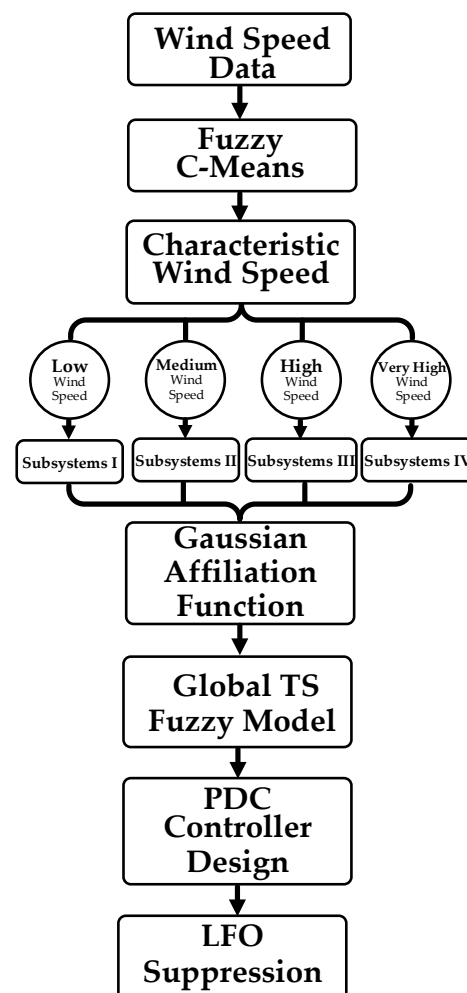


Figure 1. The flowchart of the research methodology.

3.2. System Description

The simplified power system model with DFIGs is presented in Figure 2, which consists of several SGs in area A and area B and a DFIG wind farm. The dynamic equations

between the equivalent centers of inertia of the SGs of area A and area B within the system can be expressed as [38]

$$\frac{d\omega_{AB}}{dt} = \frac{1}{M_A}(P_A - P_{At} + P_w) - \frac{1}{M_B}(P_B - P_{Bt}) \quad (9)$$

$$\frac{d\delta_{AB}}{dt} = \omega_{AB} \quad (10)$$

where δ_{AB} denotes the difference in swing angle between areas A and B ; ω_{AB} indicates the difference in angle speeds between the centers of inertia of the two areas; P_{At} is the active power transferred from bus A to bus B ; P_{Bt} is the active power transferred from bus B to area B ; P_A denotes total power generation in area A ; P_B denotes the total power consumption of area B ; and M_A and M_B represent the equivalent inertial time constant for each of the two areas.

$$P_{At} = P_{Bt} = \frac{U_A U_B \sin \delta_{AB}}{[X_{At} + X_{Bt} + X_L] + [X_{At} X_{Bt} + X_{At} X_L]/X_D} \quad (11)$$

where U_A denotes the phase voltage of buses A ; U_B denotes the phase voltage of buses B ; X_{At} and X_{Bt} represent the equivalent reactance; X_L is the equivalent line reactance; and X_D is the dynamic reactance of the reactive power of the wind farm, and its magnitude can be evaluated by

$$X_D = -\frac{U_A^2}{Q_D} \quad (12)$$

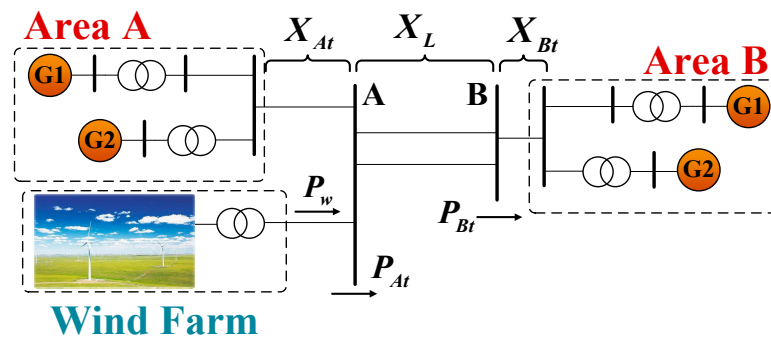


Figure 2. Two-area power system with DFIGs.

When the system can maintain stability or operates with small vibrations, $\sin \delta_{AB}$ becomes small enough to be approximated as δ_{AB} . Combining Equations (11) and (12), the active power P_{At} and P_{Bt} can be expressed as follows:

$$P_{At} = P_{Bt} = \frac{U_A U_B \sin \delta_{AB}}{[X_{At} + X_{Bt} + X_L] - [X_{At} X_{Bt} + X_{At} X_L] U_A^2 / X_D Q_D} \approx k \delta_{AB} \quad (13)$$

where k represents the coefficient relationship between δ_{AB} and P_A/P_B .

Equations (9), (10), and (13) can be transformed into the system state space equations as

$$\begin{cases} \dot{x} = Ax + Bu + C \\ y = x \end{cases} \quad (14)$$

where

$$x = \begin{bmatrix} x_1 \\ x_2 \end{bmatrix} = \begin{bmatrix} \omega_{AB} \\ \delta_{AB} \end{bmatrix}, \quad \dot{x} = \begin{bmatrix} \dot{x}_1 \\ \dot{x}_2 \end{bmatrix} = \begin{bmatrix} \dot{\omega}_{AB} \\ \dot{\delta}_{AB} \end{bmatrix}, \quad u = P_w$$

$$A = \begin{bmatrix} & k \\ 1 & \end{bmatrix} = \begin{bmatrix} \frac{U_A U_B}{[X_{At} + X_{Bt} + X_L] - \frac{[X_{At} X_{Bt} + X_{At} X_L] U_A^2}{X_D Q_D}} \\ 1 \end{bmatrix}$$

$$B = \begin{bmatrix} \frac{1}{M_A} \\ 0 \end{bmatrix}, C = \begin{bmatrix} \frac{P_A}{M_A} - \frac{P_B}{M_B} \\ 0 \end{bmatrix}$$

3.3. Structural Identification Based on Fuzzy C-Mean Arithmetic

FCMA is a fusion of clustering algorithms and fuzzy theory, serving as an extension of traditional hard clustering techniques. The core concept of FCMA is to calculate the degree of affiliation between the sample points and each cluster center and classify the sample points under the cluster center with the highest degree of affiliation. In traditional modeling, the TS model normally selects the upper and lower boundaries of the nonlinear system as the fuzzy sets, i.e., the determined principle based on the sector linearization is applied. However, the operational state of the DFIG varies with wind speed, and adopting the boundaries of the system as a fuzzy set leads to excessive data loss, which leads to degradation of the model fit and affects the LFO damping effect. To solve this problem, a fuzzy set-determined principle based on FCMA is proposed in this paper, which clusters the daily average wind speed data from wind farms by using the obtained wind speed clustering centers as fuzzy sets for the TS model. Compared with sector linearization, the proposed method is able to improve the fit of the TS model by retaining the data of the actual working conditions of the wind farm without increasing the number of fuzzy sets significantly. Therefore, the corresponding system states under each fuzzy set of the proposed TS model are closer to the actual operating state, which further improves the fitting ability of the proposed TS model for DFIG-based power systems.

Set the wind speed sample dataset of the wind farm as $V = \{v_1, v_2, \dots, v_n\}$, the affiliation matrix as $U = [u_{ij}]_{k \times n}$, and the wind speed clustering center as $V_C = [V_{C1}, V_{C2}, \dots, V_{Ck}]^T$.

The objective function of the FCMA is given as follows:

$$\begin{cases} \min \left\{ J(A, V_{C1}, V_{C2}, \dots, V_{Ck}) = \sum_{i=1}^k \sum_{j=1}^n u_{ij}^m d_{ij}^2 \right\} \\ \text{s.t. } \sum_{i=1}^k u_{ij} = 1, u_{ij} \in [0, 1], \forall j = 1, 2, \dots, n \end{cases} \quad (15)$$

where k denotes the number of wind speed clustering centers; n is the number of samples of the daily average wind speed at the wind farm; m represents the weight index affecting the affiliation matrix; u_{ij} represents the degree of affiliation of the j th daily mean wind speed to the i -th wind speed clustering centers; and $d_{ij} = \|V_{Ci} - v_j\|$ is the distance between the j -th daily mean wind speed and the i -th wind speed clustering center.

The function is constructed by adding Lagrange multipliers $\lambda = [\lambda_1, \dots, \lambda_n]$ to the n constraints in Equation (15) as

$$J = \sum_{i=1}^k \sum_{j=1}^n u_{ij}^m d_{ij} + \sum_{j=1}^n \lambda_j \left(\sum_{i=1}^k u_{ij} - 1 \right) \quad (16)$$

The partial derivatives of V_{Ci} and u_{ij} in Equation (16) can be obtained as follows:

$$\frac{\partial J}{\partial V_{Ci}} = \sum_{i=1}^k \sum_{j=1}^n \frac{\partial u_{ij}^m d_{ij}}{\partial V_{Ci}} + \frac{\partial \sum_{j=1}^n \lambda_j \left(\sum_{i=1}^k u_{ij} - 1 \right)}{\partial V_{Ci}} \quad (17)$$

$$= \sum_{i=1}^k \sum_{j=1}^n \frac{\partial u_{ij}^m d_{ij}}{\partial V_{Ci}} = u_{ij}^m \sum_{j=1}^n \frac{\partial d_{ij}}{\partial V_{Ci}} = \sum_{j=1}^n u_{ij}^m V_{Ci} - \sum_{j=1}^n u_{ij}^m v_j$$

$$\begin{aligned} \frac{\partial J}{\partial u_{ij}} &= \sum_{j=1}^n \sum_{i=1}^k m u_{ij}^{m-1} d_{ij} + \sum_{j=1}^n k \lambda_j \\ &= \sum_{j=1}^n \left(\sum_{i=1}^k m u_{ij}^{m-1} d_{ij} + k \lambda_j \right) = \sum_{j=1}^n \sum_{i=1}^k (m u_{ij}^{m-1} d_{ij} + \lambda_j) \end{aligned} \quad (18)$$

Let Equations (17) and (18) equal to zero, then the wind speed cluster centers V_{ci} and membership degrees u_{ij} can be calculated as

$$V_{ci} = \frac{\sum_{j=1}^n u_{ij}^m v_j}{\sum_{j=1}^n u_{ij}^m} \quad (19)$$

$$u_{ij} = \frac{1}{\sum_{p=1}^k \left(\frac{d_{ij}}{d_{pj}} \right)^{\frac{m}{m-1}}} \quad (20)$$

Assuming a random generation of a set of wind speed cluster centers and membership matrices, the wind speed cluster centers are obtained by iterating Equations (19) and (20) until the algorithm converges. The detailed steps to obtain wind speed clustering centers by adopting the FCMA are presented in Figure 2.

The Weibull two-parameter distribution function is taken to generate the daily mean wind speed sample data,

$$f(v) = \frac{w}{c} \left(\frac{v}{c} \right)^{w-1} \exp \left(- \left(\frac{v}{c} \right)^w \right) \quad (21)$$

where v is the wind speed; w denotes shape parameter (dimensionless); and c represents the scale parameter.

The probabilistic model Equation (21) is used to randomly generate 365 daily average wind speeds for simulating the working conditions of DFIG in a real world. The FCMA shown in Figure 3 is performed by setting the number of wind speed clustering centers as $k = 4$, the weighting factor as $m = 2$, the maximum number of iterations as $n = 10^6$ and the stop-iteration threshold as $\varepsilon = 10^{-6}$. Equations (19) and (20) are used to calculate the objective function J , which consists of the daily average wind speed, the affiliation matrix, and the wind speed clustering centers. The iteration is stopped when the stopping condition is satisfied, and the wind speed clustering center will be obtained. As shown in Figure 4, the clustering centers obtained by FCMA for the randomly generated wind speeds are

$$V_c = [V_{c1} \ V_{c2} \ V_{c3} \ V_{c4}] = [3.8674 \ 6.7776 \ 9.2881 \ 12.3493] \quad (22)$$

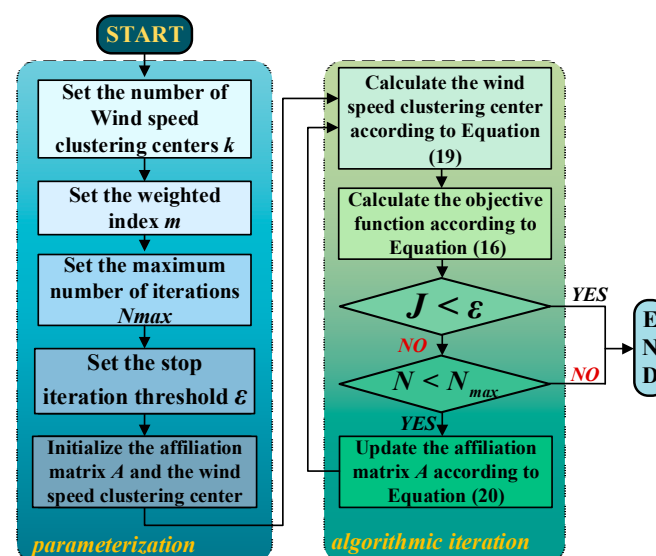


Figure 3. Flowchart of FCMA clustering algorithm.

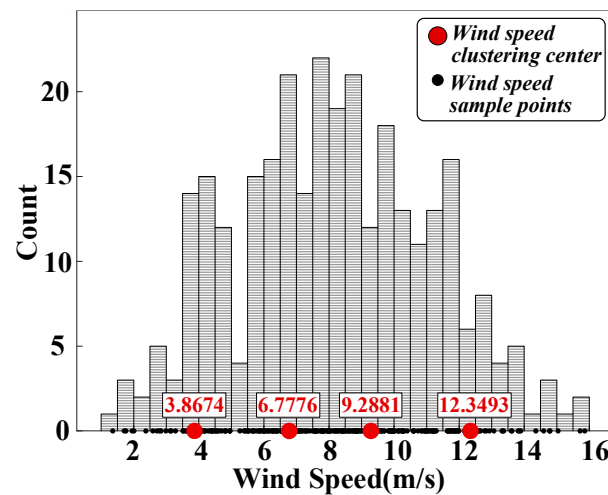


Figure 4. Wind speed distribution.

3.4. TS Fuzzy Model

The equivalent reactance X_D of the DFIG from Equation (12) is related to the bus voltage U_A and the reactive power Q_D of the DFIG. Therefore, as the U_A and Q_D shows oscillation during LFO, the state matrix in the system undergoes a nonlinear change. In addition, the system state equation is altered due to the change in the operating state of the DFIG at different wind speeds. Based on the above two situations, the state equations of the DFIG-based power systems are constantly changing during LFO, which makes the traditional control strategies ineffective in suppressing LFO. To solve this problem, a control strategy adopting TS fuzzy modeling is proposed, which addresses the nonlinear changes in the system under LFO by utilizing the superior approximation ability of the TS fuzzy model in the nonlinear system. Additionally, the wind speed clustering centers obtained through FCMA are used as the fuzzy sets of the TS fuzzy model to deal with the variation of the system at different wind speeds. Moreover, since the TS fuzzy system is represented by the input–output relationships of the system, this enables the model to be rapidly updated by the state matrix when the renewable energy equipment is increased in the system. This feature improves the issue of model misalignment in conventional modeling when the system changes. Further, since the issue of accurate modeling inside the system is not involved, the TS fuzzy model can still show well-fitting capability in the face of ultra-large-scale power systems, which cannot be achieved by the traditional modeling methods. An overview of the overall modeling concept and control strategy is shown in Figure 5.

The DFIG-based power system can be described by fuzzy rules for system input–output relationships.

Model Rule i :

$$\begin{aligned} &\text{IF } z_{i1}(t) \text{ is } M_{i1} \text{ and } \dots, z_{ip}(t) \text{ is } M_{ip} \\ &\text{Then } \begin{cases} \dot{\mathbf{x}}(t) = \mathbf{A}_i \mathbf{x}(t) + \mathbf{B}_i \mathbf{u}(t) + \mathbf{C}_i, \\ \mathbf{y}(t) = \mathbf{x}(t), \end{cases} \quad i = 1, 2, \dots, k \end{aligned} \quad (23)$$

where z_{ip} is the premise variable; M_{ip} is the fuzzy set; $\mathbf{x}(t)$ denotes the state vector; $\mathbf{u}(t)$ represents the input vector; $\mathbf{y}(t)$ represents the output vector; p denotes the number of fuzzy sets; and k denotes the number of model rules.

Gaussian membership function is utilized as the membership function in the TS fuzzy model, as given by

$$\mu_{ij}(v_j) = e^{-\frac{(v_j - V_{ci})^2}{2\sigma^2}}, \quad i, j = 1, 2, \dots, k \quad (24)$$

where $\mu_{ij}(v_j)$ denotes the membership of parameter v_j to the fuzzy set V_{ci} ; V_{ci} is the distributional expectation as well as the wind speed clustering center; and σ represents

the width of the Gaussian affiliation function. The fuzzy membership degree is shown in Figure 6.

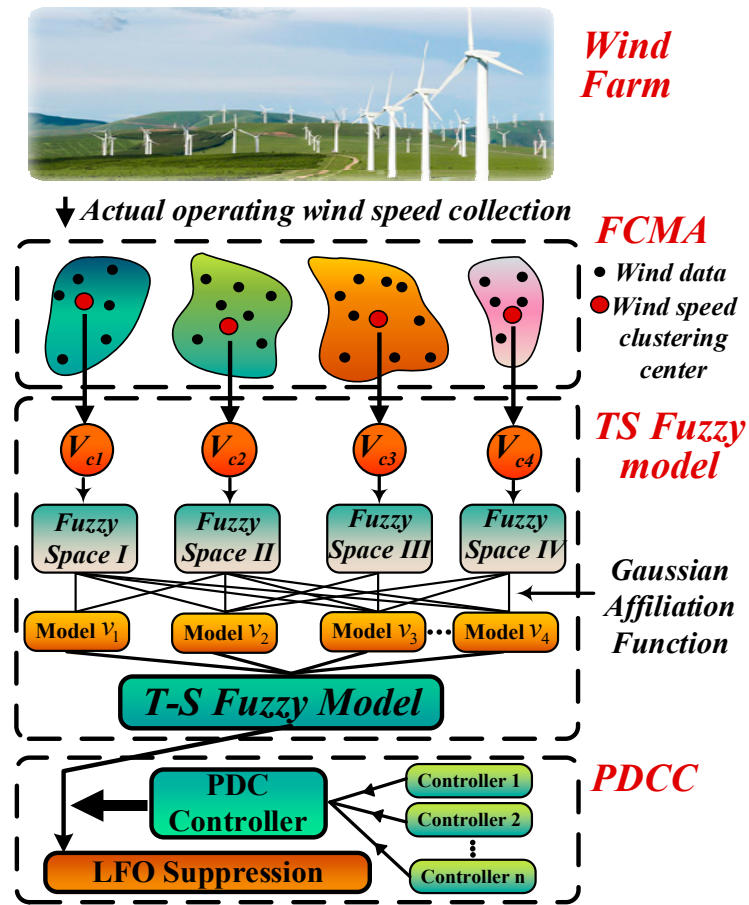


Figure 5. TS model oscillation suppression strategy based on FCMA premise variable processing.

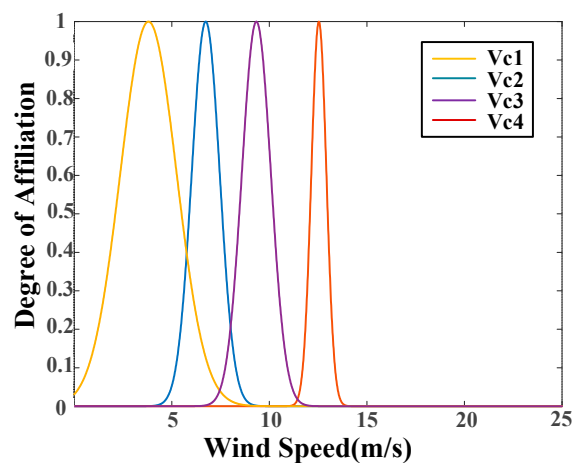


Figure 6. Membership function.

Then, the whole model of the TS fuzzy model of a DFIG-based power system is given as

$$\dot{x}(t) = A_s x(t) + B_s u(t) + C_s \quad (25)$$

where

$$A_s = \sum_{i=1}^k h_i(\rho(t)) A_i, \quad B_s = \sum_{i=1}^k h_i(\rho(t)) B_i \quad (26)$$

$$h_i(z(t)) = \frac{w_i(\rho(t))}{\sum_{i=1}^k w_i(\rho(t))}, w_i(\rho(t)) = \prod_{j=1}^p \mu_{ij}(\rho(t)) \quad (27)$$

$$h_i(\rho(t)) \geq 0, i = 1, 2, \dots, k, \sum_{i=1}^k h(\rho(t)) = 1 \quad (28)$$

Adopting the wind speed clustering center obtained from Equation (22) as the premise variable of Equation (25), we have

$$R^i: \text{ IF } v \text{ is } V_{ci}, \text{ THEN } \begin{cases} \dot{x}(t) = A_i x(t) + B_i u(t) + C_i \\ y(t) = \dot{x}(t), \end{cases} \quad i = 1, 2, 3, 4 \quad (29)$$

Therefore, one obtains

$$\begin{aligned} A_1 &= \begin{bmatrix} 0 & -47.3781 \\ 1 & 0 \end{bmatrix}, A_2 = \begin{bmatrix} 0 & -47.8317 \\ 1 & 0 \end{bmatrix} \\ A_3 &= \begin{bmatrix} 0 & -48.5612 \\ 1 & 0 \end{bmatrix}, A_4 = \begin{bmatrix} 0 & -50.1239 \\ 1 & 0 \end{bmatrix} \\ B_i &= \begin{bmatrix} 0.1538 \\ 0 \end{bmatrix}, i = 1, 2, 3, 4 \\ C_1 &= \begin{bmatrix} 0.0405 \\ 0 \end{bmatrix}, C_2 = \begin{bmatrix} 0.0405 \\ 0 \end{bmatrix} \\ C_3 &= \begin{bmatrix} 0.0405 \\ 0 \end{bmatrix}, C_4 = \begin{bmatrix} 0.0406 \\ 0 \end{bmatrix} \end{aligned} \quad (30)$$

By applying single-point fuzzification and weighted average defuzzification to Equation (29), the following whole model is obtained:

$$\begin{cases} \dot{x}(t) = \sum_{i=1}^4 h(v) A_i x(t) + \sum_{i=1}^4 h(v) B_i u(t) + \sum_{i=1}^4 h(v) C_i \\ y(t) = \dot{x}(t) \end{cases} \quad (31)$$

4. TS Parallel Distributed Compensation Controller Design and Stability Proof

Due to the integration of a large number of DFIGs in wind farms, the power system exhibits significant nonlinear characteristics. This nonlinearity undermines the effectiveness of classical PID controllers and adaptive control strategies in suppressing LFO to varying degrees. Classical PID control is primarily designed for linear systems with fixed parameters, and although certain improved versions of PID control allow for parameter adjustment, their performance in controlling highly nonlinear systems remains inadequate, failing to meet the demands of complex power systems. On the other hand, while adaptive control strategies can dynamically adjust control parameters in response to system changes, this adjustment usually relies on complex parameter adjustment rules. In highly coupled, complex systems such as power systems with wind farm integration, adaptive control requires sophisticated control algorithms to achieve real-time parameter adjustment, rendering the design, implementation, and tuning of adaptive controllers highly intricate.

The distributed parallel compensation control based on the TS fuzzy model offers a more efficient solution. It designs local controllers for each subsystem under different fuzzy sets, and these local controllers are combined into a global controller using consistent fuzzy rules and membership functions. Each subsystem operates as a linear system under its corresponding fuzzy rule, which simplifies the design of the local controllers. During operation, the PDC controller uses membership functions to activate different local controllers according to the fuzzy rules, thus avoiding the need for the complex parameter adjustment rules required by adaptive control while delivering superior LFO suppression

performance at the local level. As a result, the TS-PDCC controller effectively addresses the requirements for LFO suppression in power systems with wind farm integration.

Linear subsystems under multiple fuzzy sets are smoothly connected by an affiliation function, which constitutes the whole system. The design principle of TS-PDCC is to design the local controllers for the subsystems under each fuzzy set separately and form a global controller with those local controllers using the same fuzzy rules and affiliation functions.

The proposed TS fuzzy model is shown in Equation (25), and since the coefficient matrix C_s remains constant, the stability of the TS fuzzy model is equivalent to the stability of the following system:

$$\dot{x}(t) = A_s x(t) + B_s u(t) \quad (32)$$

Based on the TS-PDCC design principles, the following control principles are introduced, where each rule i is

$$R^1: \text{ IF } v \text{ is } V_{ci}, \text{ THEN} \quad u(t) = \sum_{i=1}^k K_i x(t) \quad (33)$$

The global fuzzy controller is obtained as

$$u(t) = \sum_{i=1}^k h_i(v) K_i x(t) \quad (34)$$

The closed-loop system is obtained by taking the global fuzzy controller (34) into system (32):

$$\dot{x}(t) = \sum_{i=1}^k \sum_{j=1}^k h_i(v) h_j(v) (A_i + B_i K_j) x(t) \quad (35)$$

The closed-loop system (35) can be transformed as

$$\begin{aligned} \dot{x}(t) = & \sum_{i=1}^k h_i(v) h_i(v) Z_{ii} x(t) \\ & + 2 \sum_{i=1}^k \sum_{i < j} h_i(v) h_j(v) \left\{ \frac{Z_{ij} + Z_{ji}}{2} \right\} x(t) \end{aligned} \quad (36)$$

$$Z_{ij} = A_i - B_i K_j, \quad i < j \text{ s.t. } h_i \cap h_j \neq \emptyset \quad (37)$$

Theorem 1. *If the equilibrium point of the continuous fuzzy control system described by system (28) is globally asymptotically stable, then there exists a common positive definite matrix P such that the following condition holds:*

$$\begin{cases} Z_{ii}^T P + P Z_{ii} < 0 \\ \left\{ \frac{Z_{ij} + Z_{ji}}{2} \right\}^T P + P \left\{ \frac{Z_{ij} + Z_{ji}}{2} \right\} \leq 0 \end{cases} \quad (38)$$

Proof. Constructing the candidate Lyapunov function as follows:

$$V(x, v) = x^T P x \quad (39)$$

The derivative of the $V(x)$ can be achieved as

$$\dot{V}(x, v) = \dot{x}^T P x + x^T P \dot{x} \quad (40)$$

Based on Equations (36) and (37), Equation (41) can be obtained as

$$\begin{aligned}
 \dot{V}(\mathbf{x}, v) &= \sum_{i=1}^k h_i(v) h_i(v) \mathbf{x}^T(t) \mathbf{Z}_{ii}^T \mathbf{P} \mathbf{x}(t) + \sum_{i=1}^k h_i(v) h_i(v) \mathbf{x}^T(t) \mathbf{P} \mathbf{Z}_{ii} \mathbf{x}(t) \\
 &\quad + 2 \sum_{i=1}^k \sum_{i < j} h_i(v) h_j(v) \mathbf{x}^T(t) \left\{ \frac{\mathbf{Z}_{ij} + \mathbf{Z}_{ji}}{2} \right\}^T \mathbf{P} \mathbf{x}(t) \\
 &\quad + 2 \sum_{i=1}^k \sum_{i < j} h_i(v) h_j(v) \mathbf{x}^T(t) \mathbf{P} \left\{ \frac{\mathbf{Z}_{ij} + \mathbf{Z}_{ji}}{2} \right\}^T \mathbf{x}(t) \\
 &= \sum_{i=1}^k h_i(v) h_i(v) \mathbf{x}^T(t) \{ \mathbf{Z}_{ii}^T \mathbf{P} + \mathbf{P} \mathbf{Z}_{ii} \} \mathbf{x}(t) \\
 &\quad + 2 \sum_{i=1}^k \sum_{i < j} h_i(v) h_j(v) \mathbf{x}^T(t) \left\{ \left\{ \frac{\mathbf{Z}_{ij} + \mathbf{Z}_{ji}}{2} \right\}^T \mathbf{P} + \mathbf{P} \left\{ \frac{\mathbf{Z}_{ij} + \mathbf{Z}_{ji}}{2} \right\}^T \right\} \mathbf{x}(t)
 \end{aligned} \tag{41}$$

When the condition in (38) of Theorem 1 is satisfied, (42) can be obtained as

$$\dot{V}(\mathbf{x}, v) < 0 \tag{42}$$

Therefore, the controller satisfying Theorem 1 can stabilize the system asymptotically.

However, obtaining suitable controller parameters is difficult when solving the condition in (30). To overcome this problem, the condition in (38) is transformed into LMIs, which enables the parameters of the controllers to be obtained by solving LMIs. Therefore, when a large number of renewable energy devices are connected to cause variations in the TS fuzzy model, the ability to update the parameters of the TS-PDCC in real time by solving the LMIs greatly improves the generalizability of the proposed LFO suppression strategy. \square

Based on Theorem 1, Theorem 2, which satisfies the form of LMIs, is given as follows:

Theorem 2. *If the equilibrium point of the continuous fuzzy control system described by system (28) is globally asymptotically stable, then there exists a common positive definite matrix P such that the following LMIs hold:*

$$\left\{ \begin{array}{l} \left[\begin{array}{cc} Q & \Xi_{1i}^T \\ \Xi_{1i} & Q \end{array} \right] > 0 \\ \left[\begin{array}{cc} Q & \Xi_{2i}^T \\ \Xi_{2i} & Q \end{array} \right] > 0 \end{array} \right., (i = 1, 2, \dots, k) \tag{43}$$

where

$$\Xi_{1i} = A_i Q - B_i M_i, \quad \Xi_{2i} = \frac{(A_i + A_j)Q - B_i M_j - B_j M_i}{2} \tag{44}$$

$$Q = P^{-1}, M_i = K_i Q \tag{45}$$

Proof. Based on Equation (37) and Equation (38), Equation (46) can be obtained as

$$\left\{ \begin{array}{l} (A_i - B_i K_i)^T P (A_i - B_i K_i) < P \\ \left(\frac{A_i - B_i K_j + A_j - B_j K_i}{2} \right)^T P \left(\frac{A_i - B_i K_j + A_j - B_j K_i}{2} \right) < P \end{array} \right. \tag{46}$$

Multiplying the left and right sides of Equation (46) by P^{-1} , it can be described as

$$\left\{ \begin{array}{l} (A_i P^{-1} - B_i K_i P^{-1})^T P (A_i P^{-1} - B_i K_i P^{-1}) < P^{-1} \\ P^{-1} \left(\frac{A_i P^{-1} - B_i K_j P^{-1} + A_j P^{-1} - B_j K_i P^{-1}}{2} \right)^T P \\ \left(\frac{A_i P^{-1} - B_i K_j P^{-1} + A_j P^{-1} - B_j K_i P^{-1}}{2} \right) P^{-1} < P^{-1} \end{array} \right. \tag{47}$$

Based on Equation (45) and Equation (47), Equation (48) can be achieved as

$$\begin{cases} Q - (A_i Q - B_i M_i)^T Q^{-1} (A_i Q - B_i M_i) > 0 \\ Q - \left(\frac{(A_i + A_j)Q - B_i M_j - B_j M_i}{2} \right)^T Q^{-1} \\ \left(\frac{(A_i + A_j)Q - B_i M_j - B_j M_i}{2} \right) > 0 \end{cases} \quad (48)$$

According to Schur's complementarity theorem, Equation (48) can be transformed into the following LMIs:

$$\begin{cases} \begin{bmatrix} Q & (A_i Q - B_i M_i)^T \\ (A_i Q - B_i M_i) & Q \end{bmatrix} > 0 \\ \begin{bmatrix} Q \\ \left(\frac{(A_i + A_j)Q - B_i M_j - B_j M_i}{2} \right) \\ \left(\frac{(A_i + A_j)Q - B_i M_j - B_j M_i}{2} \right)^T \\ Q \end{bmatrix} > 0 \end{cases} \quad (49)$$

Hence, the LMIs (49) are equivalent to condition (38), i.e., the TS-PDCC parameters K_i that satisfy the LMIs (43) can make the system (31) asymptotically stable. After establishing the TS model, the TS-PDCC parameter K_i can be obtained by directly solving the LMIs, which reduces the difficulty of controller design.

Compared to suppression schemes employing PSS and POD devices, the proposed control strategy suppresses LFO by controlling the active power output of the DFIG through TS-PDCC, significantly reducing financial investment. Additionally, when the DFIG is connected to the grid or when the grid topology changes, TS-PDCC can update the state matrix according to the system changes, form new LMIs, and quickly solve for the updated control parameters. This ensures the suppression of LFO in continuously expanding power systems, which is difficult to achieve with traditional damping control. \square

5. Simulation Verification

In order to verify the effectiveness of the TS fuzzy model based on FCMA in LFO suppression, a typical two-area, four-machine power system from the IEEE database (Figure 7) is utilized to analyze the LFO suppression in a power system with DFIG penetration.

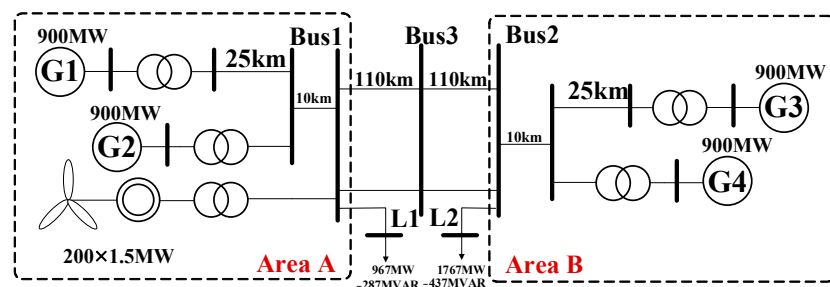


Figure 7. IEEE two-area system with DFIG.

Two SGs with a capacity of 900 MW and 200×1.5 MW DFIGs are located in area A, and two synchronous generators with a capacity of 900 MW are located in area B in the system. It is assumed that all turbines have the same operating condition and are regarded as a clustered DFIG turbine with a capacity of 200×1.5 MW.

The control scheme of TS-PDCC in the DFIG control system is shown in Figure 8, where P_{ref} denotes the output of the TS-PDCC, serving as an additional control of the q -axis rotor-side voltage of the DFIG. The simulations in the proposed study were all based on MATLAB 2022b/Simulink.

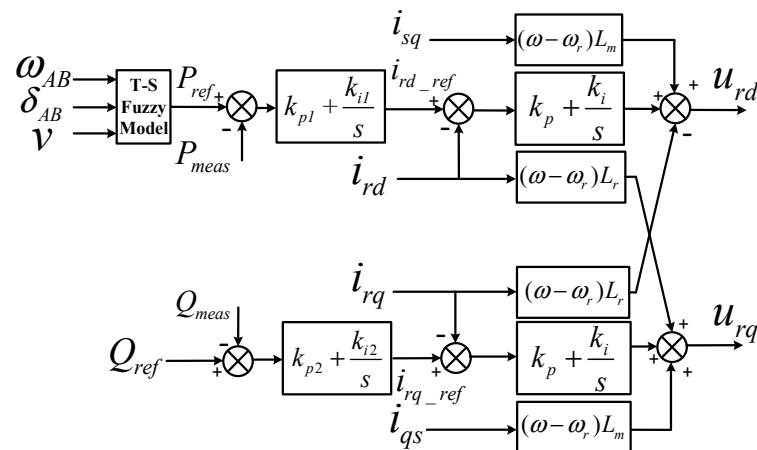


Figure 8. Configuration of TS-PDCC scheme of DFIG.

By solving the LMIs (Equation (35)), the following feedback matrix is obtained:

$$\begin{aligned} K_1 &= \begin{bmatrix} 13 & -294.9577 \end{bmatrix} & K_2 &= \begin{bmatrix} 13 & -297.9061 \end{bmatrix} \\ K_3 &= \begin{bmatrix} 13 & -302.6480 \end{bmatrix} & K_4 &= \begin{bmatrix} 13 & -312.8051 \end{bmatrix} \end{aligned} \quad (50)$$

5.1. Three-Phase Short-Circuit Fault Analysis

The effectiveness of the proposed TS fuzzy control strategy based on a wind speed reception model in mitigating the oscillations caused by a three-phase short-circuit fault is evaluated in this section. In this case, the oscillation suppression performance of the proposed TS-PDCC strategy is compared with the existing four approaches, including the fuzzy control method [38], the DFIG-POD suppression strategy [39], the SG-PSS suppression strategy [11], and the Fuzzy-PID suppression strategy [40]. For the purpose of this analysis, the three-phase short-circuit fault with a duration of 0.1 s occurs at bus 3 at $t = 10$ s. The transient response of the system is shown in Figures 9–11.

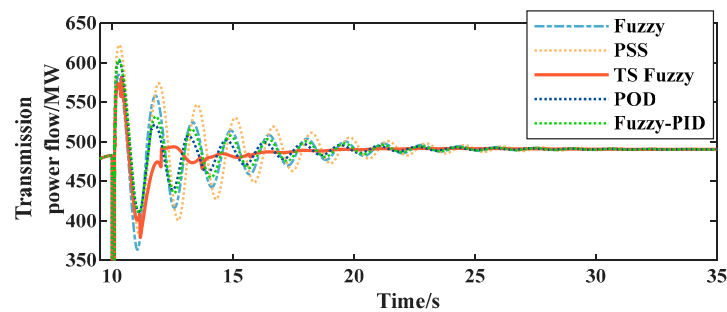


Figure 9. Response curves of active power of transmission line (Case A).

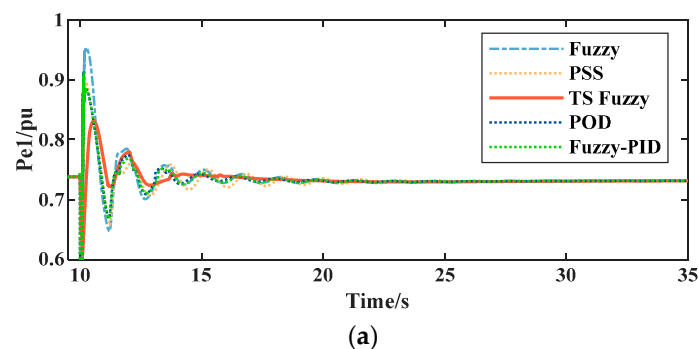


Figure 10. Cont.

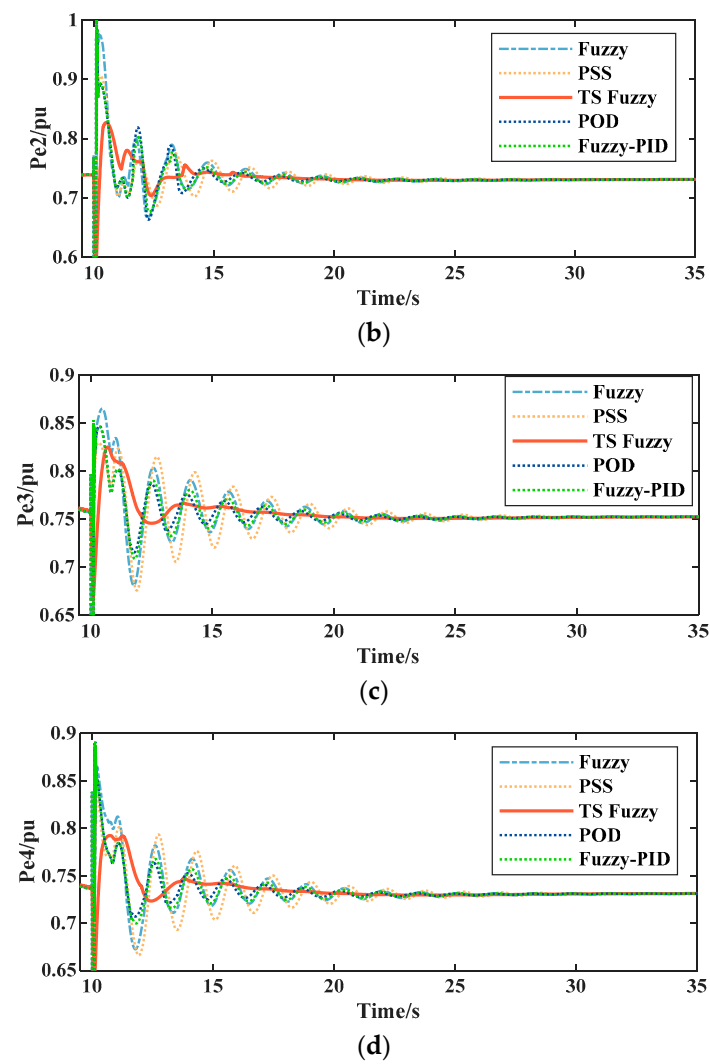


Figure 10. Synchronous generator electric power response curves (Case A). (a) SG1 electric power response curves. (b) SG2 electric power response curves. (c) SG3 electric power response curves. (d) SG4 electric power response curves.

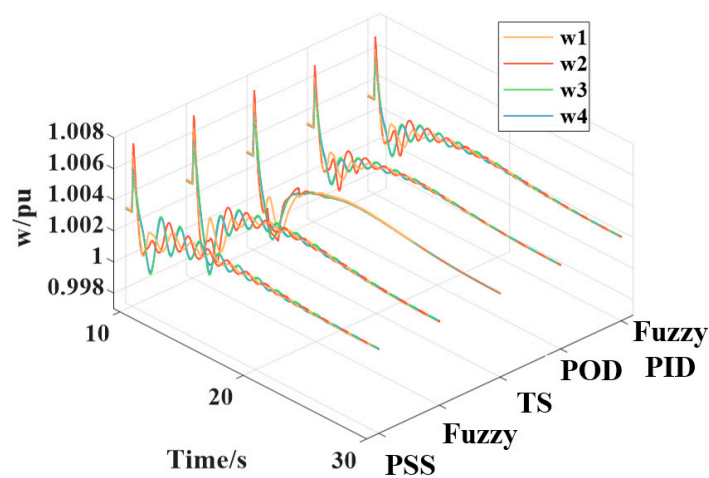


Figure 11. Speed curves of synchronous generator (Case A).

The active power oscillation curves of the transmission line between areas A and B during the occurrence of the three-phase short-circuit fault are illustrated in Figure 9. Referring to the performance indicators shown in Table 1, it can be seen that compared with the use of PSS, POD, fuzzy control, and Fuzzy-PID, the proposed control strategy significantly reduces the amplitude and duration of oscillations, shortening the settling time by 58.29%, 60.30%, 45.39%, and 38.78%, respectively.

Table 1. Performance indicator of active power oscillation suppression of transmission line.

Control Strategy		PSS	Fuzzy	TS	POD	Fuzzy-PID
Case A	Oscillation time (s)	24.414	23.624	10.183	18.648	16.633
	Overshot (%)	26.91	19.26	18.15	22.91	23.08
Case B	Oscillation time (s)	35.552	32.369	16.541	26.545	24.332
	Overshot (%)	16.60	8.88	9.66	7.84	10.44
Case C	Oscillation time (s)	26.367	19.802	12.740	20.104	22.566
	Overshot (%)	9.05	4.94	2.97	3.34	1.71

In addition, the electric power curves and rotor angular velocity response curves of four SGs in areas A and B during the three-phase short-circuit fault are shown in Figure 9 and Figure 11, respectively. From Figures 10 and 11, the amplitudes of the generator electric power and rotor angular velocity oscillations of the proposed TS-PDCC strategy are significantly reduced compared with the other four control strategies. And the oscillation time is dramatically reduced. Therefore, the proposed TS-PDCC control proved to be superior to the other suppression schemes in mitigating LFOs, thereby enhancing the stability of the wind-integrated power system under LFO conditions.

5.2. Impact of Disturbances at Synchronous Generator Terminals

In order to further investigate the performance of the proposed TS-PDCC strategy under small system disturbances, the excitation reference voltage V of the SG2 drops from 1 p.u to 0.9 p.u at $t = 15$ s to create an inter-area oscillation. The oscillation suppression performance of the proposed TS-PDCC strategy is compared with the other four control strategies. The transient response of the system is shown in Figures 12–14.

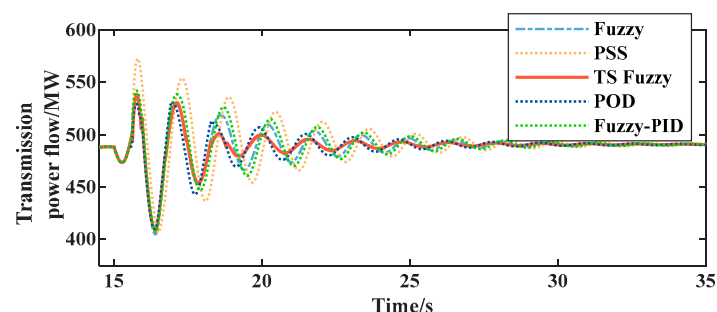


Figure 12. Response curves of active power of transmission line (Case B).

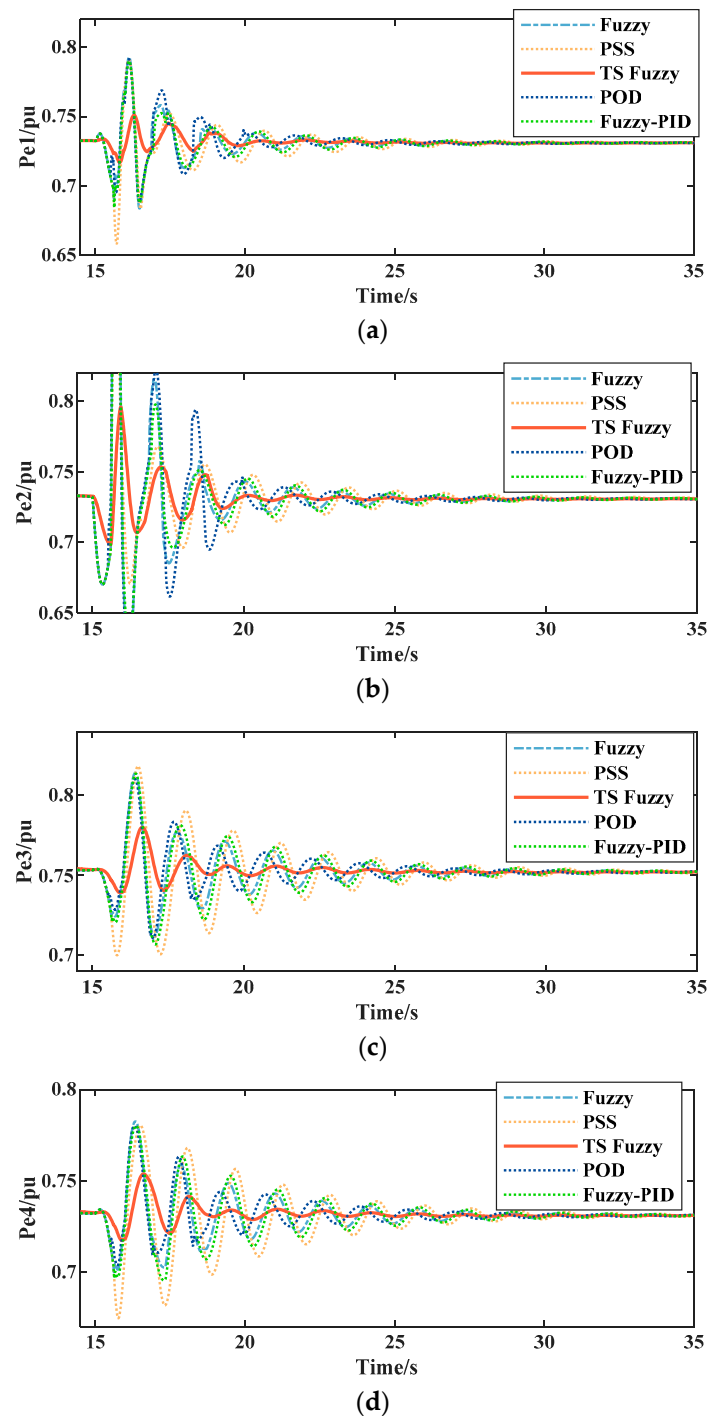


Figure 13. Synchronous generator electric power response curves (Case B). (a) SG1 electric power response curves. (b) SG2 electric power response curves. (c) SG3 electric power response curves. (d) SG4 electric power response curves.

The active power oscillation curves and the oscillation time of the transmission lines between areas A and B under generator disturbance are presented in Figure 12 and Table 1, respectively. Referring to the performance indicators shown in Table 1, it can be seen that compared with the use of PSS, POD, fuzzy control, and Fuzzy-PID, the proposed control strategy significantly reduces the amplitude and duration of oscillations, shortening the settling time by 53.47%, 37.69%, 48.90%, and 44.35%, respectively.

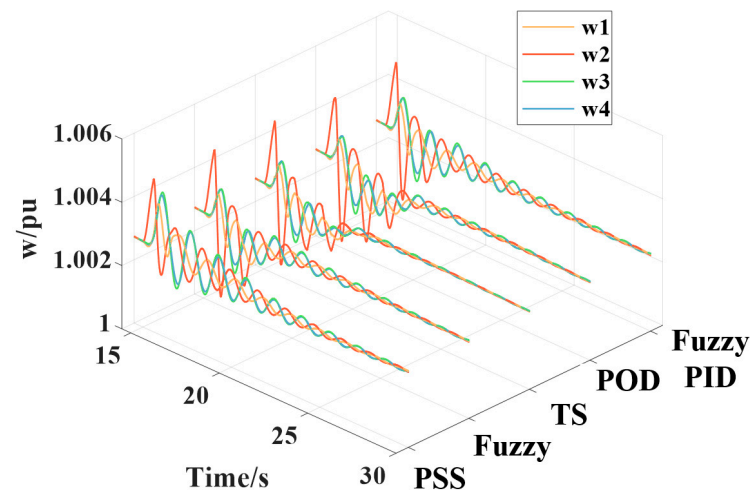


Figure 14. Speed curves of synchronous generator (Case B).

Additionally, by comparing the electric power curves of the SG (Figure 13) and the rotor angular velocity response curves (Figure 14), the oscillation amplitude and duration are greatly reduced under the proposed TS-PDCC strategy. Therefore, it has been proven that the proposed TS-PDCC control outperforms the four compared suppression schemes in mitigating LFO, thereby enhancing the stability of the wind energy-integrated power system under LFO conditions.

5.3. Perturbation Analysis with Sudden Load Change

In this case, the robustness against load variation of the proposed control strategy is validated. In the simulation, load L1 is increased to 1467 MW at $t = 10$ s and is recovered at $t = 10.1$ s. The transient response of the system is shown in Figures 15–17.

The active power oscillation curves and quantitative performance of the transmission line between areas A and B under load disturbances are presented in Figure 15 and Table 1, from which it can be seen that the system can achieve stability within 12.740 s under the proposed TS-PDCC strategy. However, the durations of oscillation with the other control strategies are 26.367 s, 19.802 s, 20.104 s, and 22.566 s, respectively.

From the electric power curves of four SGs (Figure 16) and the rotor angular velocity response curves under the five types of control methods (Figure 17), it can be obtained that the generator electric power and the rotor angular velocity under the proposed TS fuzzy control can realize stability with shorter time and smaller amplitude. Compared to existing oscillation suppression strategies, the proposed control method is more effective in suppressing inter-area oscillations caused by load variations.

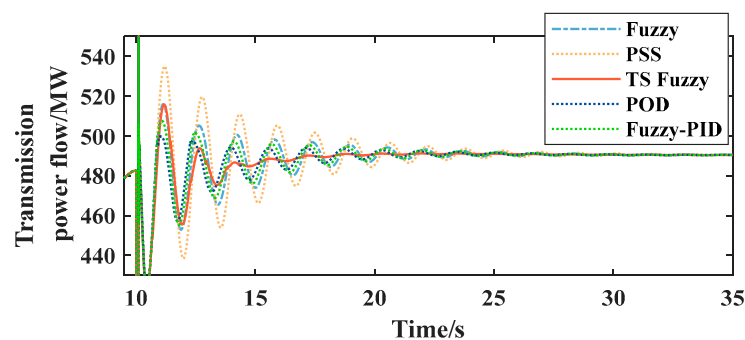


Figure 15. Response curves of active power of transmission line (Case C).

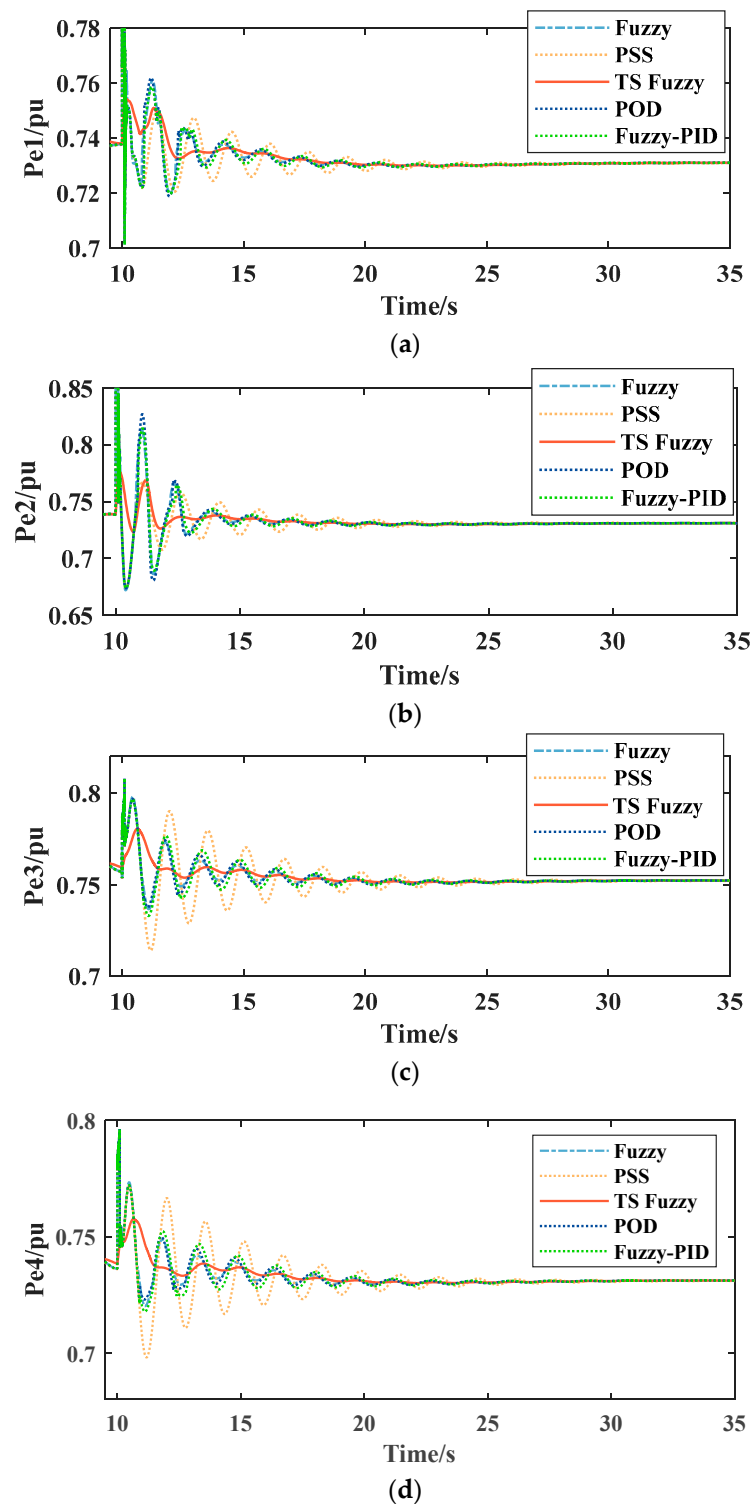


Figure 16. Synchronous generator electric power response curves (Case C). (a) SG1 electric power response curves. (b) SG2 electric power response curves. (c) SG3 electric power response curves. (d) SG4 electric power response curves.

As shown in Figure 18, comparison results of the convergence time indicate that the proposed control strategy has better suppression performance on the LFO caused by various faults in the power system. Therefore, the superiority of the proposed TS-PDCC strategy during LFO in multiple cases is verified.

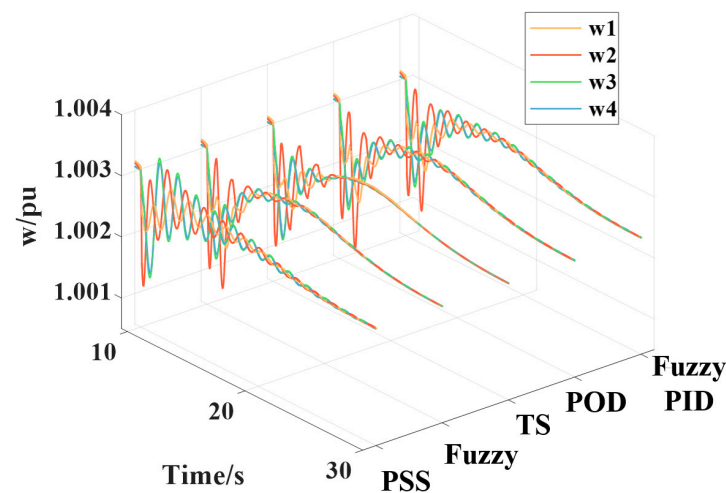


Figure 17. Speed curves of synchronous generator (Case C).

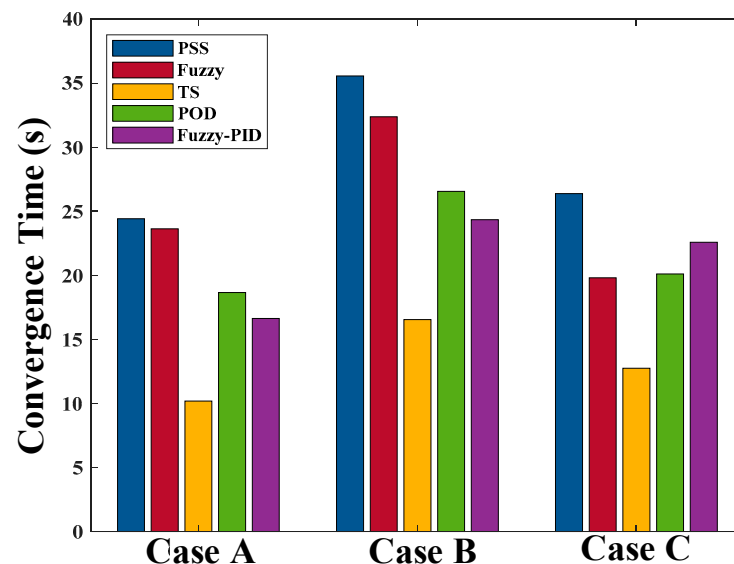


Figure 18. Transmission line oscillation convergence time comparison.

6. Conclusions

By scrutinizing the power system equation incorporating a DFIG with TS fuzzification and employing FCMA for processing wind speed data derived from wind farms, this paper presents a TS fuzzy model, TS-PDCC, that relies on FCMA premise variable processing to regulate the active power output of the wind turbine and to mitigate inter-area low-frequency oscillations in DFIG-integrated systems. By integrating DFIG-based WTs into the classic IEEE benchmark system, the overall suppression performance of the proposed TS-PDCC control, along with the conventional damping control strategy, is compared. Three case studies are conducted under different operation scenarios, i.e., a short-circuit fault happening in the transmission line, a perturbation of the power output of SGs, and sudden load side changes. The simulation results have shown that the proposed TS-PDCC approach outperforms the traditional damping method in response velocity, oscillation overshoot, and computational efficiency.

The limitations of the proposed TS-PDCC strategy are as follows: In the current approach, all wind turbines in the wind farm are considered to operate under the same conditions. However, due to the wake effect, the total active power generated by the wind farm is actually lower than the theoretical value under different wind directions, resulting in a control dead zone when using the active power of the wind farm for LFO suppression, which affects the control performance. Additionally, the establishment of fuzzy rules only

takes wind speed into account, neglecting other factors such as wind direction, which may reduce the accuracy of the TS fuzzy model in fitting the system. Furthermore, the subsystems under each fuzzy set still rely on state equations, which increases the difficulty of subsystem modeling when dealing with more complex systems.

Based on these limitations, future research could include but is not limited to the following: developing a multi-directional wind farm model that accounts for the wake effect to reduce the weakening of LFO suppression caused by the control dead zone; incorporating multiple factors, such as wind direction, into fuzzy set partitioning to improve the system's fitting accuracy; and using artificial intelligence techniques to identify subsystem models, thereby reducing the modeling complexity and avoiding the challenges of solving controllers caused by an excessive number of fuzzy rules.

Author Contributions: Conceptualization, R.S. and S.H.; methodology, S.H. and L.X.; software, R.S. and Y.Z.; validation, Y.Z. and R.S.; formal analysis, P.T.; investigation, P.T.; resources, L.X.; data curation, T.L.; writing—original draft preparation, R.S.; writing—review and editing, R.S. and S.H.; visualization, Z.S.; supervision, Y.Z.; project administration, S.H.; funding acquisition, L.X. All authors have read and agreed to the published version of the manuscript.

Funding: This work was supported by the Scientific Research Foundation of Hunan Provincial Education Department under Grant 23B0297; National Natural Science Foundation of China (No. 52377074, No. 52007015); Chongqing Municipal Technology Innovation and Application Development Special Key Project under Grant CSTB2023TIAD-KPX0088.

Data Availability Statement: Data are available upon request.

Conflicts of Interest: The authors declare no conflicts of interest.

Abbreviations

Acronym	Full Term
DFIG	Doubly fed induction generator
FCMA	Fuzzy C-mean algorithm
LFO	Low-frequency oscillation
LMI	Linear Matrix Inequality
POD	Power oscillation damper
PSS	Power system stabilizer
RES	Renewable energy source
SG	Synchronous generator
TS-PDCC	TS parallel distributed compensation control

References

- Hajimineh, R.; Rastegarnia, G. The outlook of global power from an energy policy perspective. *Open Energy Rev.* **2024**, *48*, 167–178. [\[CrossRef\]](#)
- Kim, W.W.; Shin, J.S.; Kim, J.O. Operation Strategy of Multi-Energy Storage System for Ancillary Services. *IEEE Trans. Power Syst.* **2017**, *32*, 4409–4417. [\[CrossRef\]](#)
- Muhtadi, A.; Pandit, D.; Nguyen, N.; Mitra, J. Distributed Energy Resources Based Microgrid: Review of Architecture, Control, and Reliability. *IEEE Trans. Ind. Appl.* **2021**, *57*, 2223–2235. [\[CrossRef\]](#)
- Kroposki, B.; Johnson, B.; Zhang, Y.; Gevorgian, V.; Denholm, P.; Hodge, B.-M.; Hannegan, B. Achieving a 100% Renewable Grid. *IEEE Power Energy Mag.* **2017**, *15*, 61–73. [\[CrossRef\]](#)
- Wu, X.; Xu, S.; Shi, X.; Shahidehpour, M.; Wang, M.; Li, Z. Mitigating Subsynchronous Oscillation Using Model-Free Adaptive Control of DFIGs. *IEEE Trans. Sustain. Energy* **2023**, *14*, 242–253. [\[CrossRef\]](#)
- Nian, H.; Song, Y. Direct Power Control of Doubly Fed Induction Generator under Distorted Grid Voltage. *IEEE Trans. Power Electron.* **2014**, *29*, 894–905. [\[CrossRef\]](#)
- Gautam, D.; Vittal, V.; Harbour, T. Impact of Increased Penetration of DFIG based Wind Turbine Generators on Transient and Small Signal Stability of Power Systems. In Proceedings of the IEEE-Power-and-Energy-Society General Meeting, Minneapolis, MN, USA, 25–29 July 2010.
- Golpîra, H.; Seifi, H.; Messina, A.R.; Haghifam, M.R. Maximum Penetration Level of Micro-Grids in Large-Scale Power Systems: Frequency Stability Viewpoint. *IEEE Trans. Power Syst.* **2016**, *31*, 5163–5171. [\[CrossRef\]](#)
- Yu, Y.; Grijalva, S.; Thomas, J.J.; Xiong, L.; Ju, P.; Min, Y. Oscillation Energy Analysis of Inter-Area Low-Frequency Oscillations in Power Systems. *IEEE Trans. Power Syst.* **2016**, *31*, 1195–1203. [\[CrossRef\]](#)

10. Sui, X.; Tang, Y.; He, H.; Wen, J. Energy-Storage-Based Low-Frequency Oscillation Damping Control Using Particle Swarm Optimization and Heuristic Dynamic Programming. *IEEE Trans. Power Syst.* **2014**, *29*, 2539–2548. [\[CrossRef\]](#)
11. Kundur, P.; Balu, N.J.; Lauby, M.G. *Power System Stability and Control*; McGraw-hill: New York, NY, USA, 1994.
12. Imran, R.M.; Hussain, D.M.A.; Soltani, M. DAC to Mitigate the Effect of Periodic Disturbances on Drive Train using Collective Pitch for Variable Speed Wind Turbine. In Proceedings of the IEEE International Conference on Industrial Technology (ICIT), Seville, Spain, 17–19 March 2015.
13. Du, W.; Chen, X.; Wang, H. Impact of Dynamic Interactions Introduced by the DFIGs on Power System Electromechanical Oscillation Modes. *IEEE Trans. Power Syst.* **2017**, *32*, 4954–4967. [\[CrossRef\]](#)
14. Chi, Y.; Tang, B.; Hu, J.; Tian, X.; Tang, H.; Li, Y.; Sun, S.; Shi, L.; Shuai, L. Overview of mechanism and mitigation measures on multi-frequency oscillation caused by large-scale integration of wind power. *CSEE J. Power Energy Syst.* **2019**, *5*, 433–443.
15. Du, W.; Bi, J.; Cao, J.; Wang, H. A Method to Examine the Impact of Grid Connection of the DFIGs on Power System Electromechanical Oscillation Modes. *IEEE Trans. Power Syst.* **2016**, *31*, 3775–3784. [\[CrossRef\]](#)
16. Domínguez-García, J.L.; Gomis-Bellmunt, O.; Bianchi, F.D.; Sumper, A. Power oscillation damping supported by wind power: A review. *Renew. Sustain. Energy Rev.* **2012**, *16*, 4994–5006. [\[CrossRef\]](#)
17. Arani, M.F.M.; Mohamed, Y. Analysis and Damping of Mechanical Resonance of Wind Power Generators Contributing to Frequency Regulation. *IEEE Trans. Power Syst.* **2017**, *32*, 3195–3204. [\[CrossRef\]](#)
18. Edrah, M.; Zhao, X.; Hung, W.; Qi, P.; Marshall, B.; Karcianas, A.; Baloch, S. Effects of POD Control on a DFIG Wind Turbine Structural System. *IEEE Trans. Energy Convers.* **2020**, *35*, 765–774. [\[CrossRef\]](#)
19. Geng, H.; Xi, X.; Liu, L.; Yang, G.; Ma, J. Hybrid Modulated Active Damping Control for DFIG-Based Wind Farm Participating in Frequency Response. *IEEE Trans. Energy Convers.* **2017**, *32*, 1220–1230. [\[CrossRef\]](#)
20. Yang, L.; Xu, Z.; Ostergaard, J.; Dong, Z.; Wong, K.; Ma, X. Oscillatory Stability and Eigenvalue Sensitivity Analysis of A DFIG Wind Turbine System. *IEEE Trans. Energy Convers.* **2011**, *26*, 328–339. [\[CrossRef\]](#)
21. Li, Y.; Li, W.; Shi, X.; Chen, X. An efficient numerical method for computing eigenvalue sensitivity with respect to operational parameters of large-scale power systems. *Electr. Power Syst. Res.* **2019**, *174*, 105859. [\[CrossRef\]](#)
22. Chau, T.; Yu, S.; Fernando, T.L.; Iu, H.; Small, M. A Novel Control Strategy of DFIG Wind Turbines in Complex Power Systems for Enhancement of Primary Frequency Response and LFOD. *IEEE Trans. Power Syst.* **2018**, *33*, 1811–1823. [\[CrossRef\]](#)
23. Khazaei, J.; Tu, Z.; Liu, W. Small-Signal Modeling and Analysis of Virtual Inertia-Based PV Systems. *IEEE Trans. Energy Convers.* **2020**, *35*, 1129–1138. [\[CrossRef\]](#)
24. AboulEla, M.E.; Sallam, A.A.; McCalley, J.D.; Fouad, A.A. Damping controller design for power system oscillations using global signals. *IEEE Trans. Power Syst.* **1996**, *11*, 767–773. [\[CrossRef\]](#)
25. Klein, M.; Rogers, G.J.; Moorthy, S.; Kundur, P. Analytical investigation of factors influencing power system stabilizers performance. *IEEE Trans. Energy Convers.* **1992**, *7*, 382–390. [\[CrossRef\]](#)
26. Surinkaew, T.; Ngamroo, I. Hierarchical Co-Ordinated Wide Area and Local Controls of DFIG Wind Turbine and PSS for Robust Power Oscillation Damping. *IEEE Trans. Sustain. Energy* **2016**, *7*, 943–955. [\[CrossRef\]](#)
27. Wong, W.; Chung, C. Coordinated Damping Control Design for DFIG-Based Wind Generation Considering Power Output Variation. *IEEE Trans. Power Syst.* **2012**, *27*, 1916–1925. [\[CrossRef\]](#)
28. Zhou, H.; Li, Q.; Lin, T.; Gao, Y.; Zhang, F.; Huang, Y.; Yang, D.; Dong, M. On Small Signal Stability Early Warning Based on Measurement Data of WAMS. In Proceedings of the Asia-Pacific Power and Energy Engineering Conference (APPEEC), Chengdu, China, 28–31 March 2010.
29. Xi, X.; Geng, H.; Yang, G.; Li, S.; Gao, F. Two-Level Damping Control for DFIG-Based Wind Farm Providing Synthetic Inertial Service. *IEEE Trans. Ind. Appl.* **2018**, *54*, 1712–1723. [\[CrossRef\]](#)
30. Ma, J.; Zhao, D.; Shen, Y. Research on Positioning Method of Low Frequency Oscillating Source in DFIG-Integrated System With Virtual Inertia Control. *IEEE Trans. Sustain. Energy* **2020**, *11*, 1693–1706. [\[CrossRef\]](#)
31. Sanniti, F.; Tzounas, G.; Benato, R.; Milano, F. Curvature-Based Control for Low-Inertia Systems. *IEEE Trans. Power Syst.* **2022**, *37*, 4149–4152. [\[CrossRef\]](#)
32. Moutevelis, D.; Roldán-Pérez, J.; Prodanovic, M.; Milano, F. Taxonomy of Power Converter Control Schemes Based on the Complex Frequency Concept. *IEEE Trans. Power Syst.* **2024**, *39*, 1996–2009. [\[CrossRef\]](#)
33. Yang, D.; Jin, E.; You, J.; Hua, L. Dynamic Frequency Support from a DFIG-Based Wind Turbine Generator via Virtual Inertia Control. *Appl. Sci.* **2020**, *10*, 3376. [\[CrossRef\]](#)
34. Huang, S.; Xiong, L.; Zhou, Y.; Gao, F.; Jia, Q.; Li, X.; Li, X.; Wang, Z.; Khan, M.W. Distributed predefined-time control for power system with time delay and input saturation. *IEEE Trans. Power Syst.* **2024**, early access. [\[CrossRef\]](#)
35. Huang, S.; Xiong, L.; Zhou, Y.; Gao, F.; Jia, Q.; Li, X.; Li, X.; Wang, Z.; Khan, M.W. Robust distributed fixed-time fault-tolerant control for shipboard microgrids with actuator fault. *IEEE Trans. Transp. Electrification* **2024**, early access. [\[CrossRef\]](#)
36. Huang, S.; Wang, J.; Huang, C.; Zhou, L.; Xiong, L.; Liu, J.; Li, P. A fixed-time fractional-order sliding mode control strategy for power quality enhancement of PMSG wind turbine. *Int. J. Electr. Power Energy Syst.* **2022**, *134*, 107354. [\[CrossRef\]](#)
37. Wang, Q.; Huang, S.; Xiong, L.; Zhou, Y.; Niu, T.; Gao, F.; Khan, M.W.; Wang, Z.; Ban, C.; Song, R. Distributed secondary control based on bi-limit homogeneity for AC microgrids subjected to non-uniform delays and actuator saturations. *IEEE Trans. Power Syst.* **2024**, early access. [\[CrossRef\]](#)

38. Li, H.; Liu, S.; Ji, H.; Yang, D.; Yang, C.; Chen, H.; Zhao, B.; Hu, Y.; Chen, Z. Damping control strategies of inter-area low-frequency oscillation for DFIG-based wind farms integrated into a power system. *Int. J. Electr. Power Energy Syst.* **2014**, *61*, 279–287. [[CrossRef](#)]
39. Li, S.; Zhang, H.; Yan, Y.; Ren, J. Parameter Optimization to Power Oscillation Damper (POD) Considering its Impact on the DFIG. *IEEE Trans. Power Syst.* **2022**, *37*, 1508–1518. [[CrossRef](#)]
40. Signe, R.K.; Motto, F.B. Fuzzy-PID controller based sliding-mode for suppressing low frequency oscillations of the synchronous generator. *Heliyon* **2024**, *10*, e35035. [[CrossRef](#)] [[PubMed](#)]

Disclaimer/Publisher’s Note: The statements, opinions and data contained in all publications are solely those of the individual author(s) and contributor(s) and not of MDPI and/or the editor(s). MDPI and/or the editor(s) disclaim responsibility for any injury to people or property resulting from any ideas, methods, instructions or products referred to in the content.